JACS
JOURNAL OF THE AMERICAN CHEMICAL SOCIETY
pubs.acs.org/JACS
Communication

A Heteroleptic Gold Hydride Nanocluster for Efficient and Selective Electrocatalytic Reduction of CO_2 to CO

Ze-Hua Gao, Kecheng Wei, Tao Wu, Jia Dong, De-en Jiang,* Shouheng Sun,* and Lai-Sheng Wang*

Cite This: *J. Am. Chem. Soc.* 2022, 144, 5258−5262
Read Online
ACCESS | Metrics & More | Article Recommendations | Supporting Information

ABSTRACT: It has been a long-standing challenge to create and identify the active sites of heterogeneous catalysts, because it is difficult to precisely control the interfacial chemistry at the molecular level. Here we report the synthesis and catalysis of a heteroleptic gold trihydride nanocluster, $[Au_{22}H_3(dppe)_3(PPh_3)_8]^{3+}$ [dppe = 1,2-bis(diphenylphosphino)ethane, PPh_3 = triphenylphosphine]. The $Au_{22}H_3$ core consists of two Au_{11} units bonded via six uncoordinated Au sites. The three H atoms bridge the six uncoordinated Au atoms and are found to play a key role in catalyzing electrochemical reduction of CO_2 to CO with a 92.7% Faradaic efficiency (FE) at −0.6 V (vs RHE) and high reaction activity (134 A/g_{Au} mass activity). The CO current density and FE_{CO} remained nearly constant for the CO_2 reduction reaction for more than 10 h, indicating remarkable stability of the $Au_{22}H_3$ catalyst. The $Au_{22}H_3$ catalytic performance is among the best Au-based catalysts reported thus far for electrochemical reduction of CO_2. Density functional theory (DFT) calculations suggest that the hydride coordinated Au sites are the active centers, which facilitate the formation of the key *COOH intermediate.

Electrochemical CO_2 reduction reaction (CO_2RR) has been considered as a very promising strategy to convert CO_2 to value-added chemcials and to balance the carbon cycle.[1,2] Gold-based nanomaterials have been one of the most widely studied catalysts for electrochemical conversion of CO_2 to CO with high selectivity and relatively low overpotentials.[3,4] Despite the tremendous progress in producing monodisperse Au nanoparticles with appreciable activity and selectivity,[5−9] their surface structure cannot be precisely resolved and well-defined, making it difficult to investigate the structure−activity relationship.[10,11] Hence, it is highly desirable to achieve synthetic control in the coordination environments of surface Au atoms to create well-defined active centers for the eluciation of the structure−activity relationship of Au nanocatalysis.

In this quest, atomically precise Au nanoclusters have attracted intensive interest because they possess high molecular purity, well-defined structures, and high surface-to-volume ratios[12−21] and have been studied as ideal model systems for understanding catalytic properties at the atomic level.[22−25] In particular, a series of thiolate-protected Au nanoclusters have been studied for CO_2RR,[26−30] although the detailed catalytic mechanisms are not well understood and are controversial.[28,31]

An ideal Au-nanocluster model catalyst should be atomically precise with uncoordinated Au (*uc*Au) sites serving as *in situ* catalytic active centers. Our focus has been on the Au_{20} pyramid, which is known to have all its atoms on the cluster surface.[32] We have tried to synthesize the Au_{20} pyramid using different phosphine ligands with the hope of creating *uc*Au sites with suitable ligands.[33−35] The use of diphosphine ligands led to the synthesis of $Au_{22}(dppo)_6$ [dppo = 1,8-bis(diphenylphosphino)octane], which was the first atom-precise Au nanocluster with 8 *uc*Au sites[36] and was found to be able to catalyze the CO oxidation reaction under mild conditions,[22] as well as being a good catalyst for H_2 activation.[37] Further investigations led to the discovery of two Au nanohydride clusters with *uc*Au, $[Au_{22}H_4(dppo)_6]^{2+}$ and $[Au_{22}H_3(dppee)_7]^{3+}$ [dppee = bis(2-diphenylphosphino)ethyl ether], where the *uc*Au sites are bridged by the H atoms.[38,39] The steric effects produced by mixed bulky ligands[40−43] provide another strategy to control the interfacial chemistry of Au nanoclusters to create catalytic active sites, which inspired us to consider mixing bidentate and monodentate phosphine ligands to try to synthesize the Au_{20} pyramid.

Here, we report the synthesis and catalysis of a new heteroleptic $[Au_{22}H_3(dppe)_3(PPh_3)_8]^{3+}$ trihydride cluster [dppe = 1,2-bis(diphenylphosphino)ethane, PPh_3 = triphenyl phosphine], when we used a mixture of dppe and PPh_3 (Figure 1a). A combination of experimental and theoretical studies revealed that the $Au_{22}H_3$ core consists of two Au_{11} units that are bonded together via two triangular faces with the three H atoms bridging six *uc*Au atoms at the interface. We have found that $[Au_{22}H_3(dppe)_3(PPh_3)_8]^{3+}$ exhibits excellent performance for the selective electrocatalytic reduction of CO_2 to CO with a 92.7% Faradaic efficiency (FE) at −0.6 V [vs reversible hydrogen electrode (RHE)], high mass activity (134 A/g_{Au}), and high stability. The catalytic performance is among the best Au-based catalysts for electrochemical reduction of CO_2 to CO. The current study demonstrates the possibility of

Received: January 19, 2022
Published: March 15, 2022

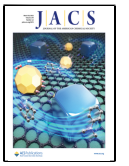

https://doi.org/10.1021/jacs.2c00725
J. Am. Chem. Soc. 2022, 144, 5258−5262

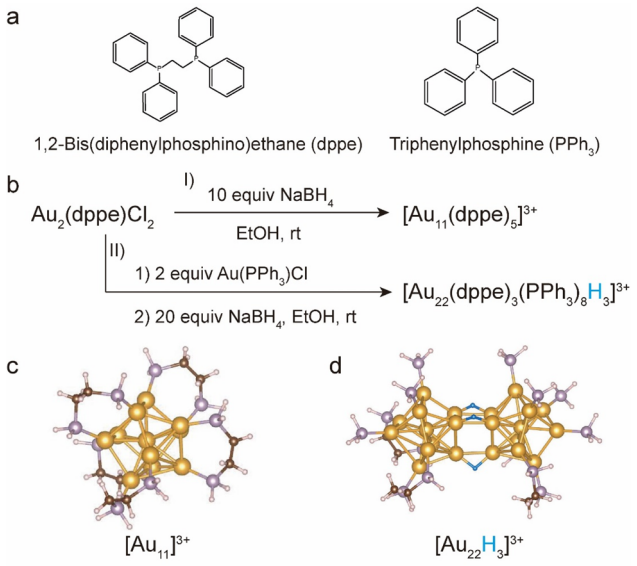

Figure 1. (a) Structures of dppe and PPh_3 ligands. (b) Synthetic routes toward (I) $[Au_{11}(dppe)_5]^{3+}$ and (II) $[Au_{22}(dppe)_3(PPh_3)_8H_3]^{3+}$. The DFT optimized structures of (c) $[Au_{11}(dppe)_5]^{3+}$ and (d) $[Au_{22}(dppe)_3(PPh_3)_8H_3]^{3+}$ clusters. Colors: Au = yellow; C = brown; P = purple; Hydride = blue; H on the ligands = white.

designing catalytically active centers using Au nanohydrides for potential applications.

The $[Au_{22}H_3(dppe)_3(PPh_3)_8]^{3+}$ cluster (abbreviated as $[Au_{22}H_3]^{3+}$ hereafter) was synthesized by reacting an excess amount of $NaBH_4$ with a mixture of $Au_2(dppe)Cl_2$ and $Au(PPh_3)Cl$ precursors, as described in Figure 1b and the Supporting Information (SI). After purification, the final product showed a distinct peak in the electrospray ionization (ESI) mass spectrum (Figure 2a, top) due to $[Au_{22}H_3]^{3+}$. To

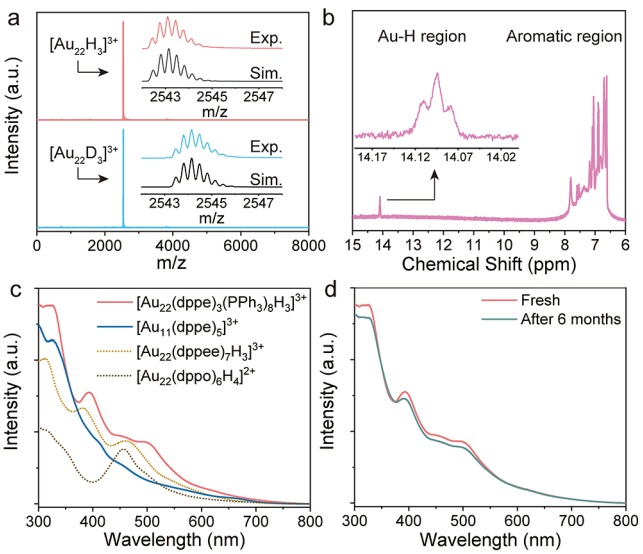

Figure 2. (a) ESI-MS spectra of $[Au_{22}H_3]^{3+}$ and $[Au_{22}D_3]^{3+}$; the insets show the experimental and simulated isotopic distributions. (b) The ^1H NMR spectrum of $[Au_{22}H_3]^{3+}$; the inset shows the enlarged signal in the Au−H region. (c) Comparison of the UV−vis absorption spectra of $[Au_{22}H_3]^{3+}$, $[Au_{11}(dppe)_5]^{3+}$, $[Au_{22}(dppee)_7H_3]^{3+}$, and $[Au_{22}(dppo)_6H_4]^{2+}$. (d) UV−vis absorption spectra of $[Au_{22}H_3]^{3+}$ solid sample stored for six months under ambient condition.

ensure that the three H atoms on $[Au_{22}H_3]^{3+}$ did not come from the ESI process, we used $NaBD_4$ instead of $NaBH_4$ to do the same reaction and obtained $[Au_{22}D_3]^{3+}$ (Figure 2a, bottom). We further characterized $[Au_{22}H_3]^{3+}$ using ^1H NMR and observed three peaks at 14.1 ppm (Figure 2b). The ratio of the integrated area for these hydride peaks to that of the 180 aromatic H atoms on the 11 phosphine ligands (6.6−7.9 ppm) is about 3:194. The observed chemical shift suggests that the three H atoms are directly bonded to Au, similar to those observed in previous Au−H nanoclusters: ~15.1 ppm in $[Au_9H(PPh_3)_8]^{2+}$,[44] ~15.5 ppm in $[Au_{22}H_4(dppo)_6]^{2+}$,[38] and ~15 ppm in $[Au_{22}H_3(dppee)_7]^{3+}$.[39] The ^{31}P NMR spectrum of the $[Au_{22}H_3]^{3+}$ cluster, however, displayed multiple peaks in the range 45−60 ppm (Figure S1), suggesting the complexity of the phosphine environments.

By performing identical syntheses using $Au_2(dppe)Cl_2$ alone, the $[Au_{11}(dppe)_5]^{3+}$ cluster [abbreviated as $[Au_{11}]^{3+}$] was obtained (Figure 1b). The corresponding ESI mass spectrum and NMR spectra were also obtained, as shown in Figures S2−S4. The results show that the sample purity is high and the phosphine environments are similar on $[Au_{11}]^{3+}$. We performed structural optimization using DFT calculations for both clusters. The optimized structures for $[Au_{11}]^{3+}$ and $[Au_{22}H_3]^{3+}$ are shown in Figure 1c and 1d, respectively. $[Au_{11}]^{3+}$ is fully capped with diphosphine ligands. However, the three H atoms bridge the six *uc*Au sites in the $[Au_{22}H_3]^{3+}$ cluster, whereas the remaining 14 surface Au atoms are coordinated by the phosphine ligands. We compared the Au−Au bond lengths between our DFT calculations and the experimental results of ($[Au_{11}(dppp)_5]^{3+}$ and $[Au_{22}(dppo)_6]^{2+}$), both agreeing well with the reported crystal data (Table S1). The $[Au_{11}]^{3+}$ cluster also shares similar bond lengths as the Au_{11} unit in the $[Au_{22}H_3]^{3+}$ cluster. More interestingly, we compared the UV−vis absorption spectra of these two clusters with those of $[Au_{22}H_3(dppee)_7]^{3+}$ and $[Au_{22}H_4(dppo)_6]^{2+}$ (Figure 2c) and found that the two $Au_{22}H_3$ clusters share similar absorption features at around 323, 394, and 446 nm. The $[Au_{11}]^{3+}$ cluster exhibits analogous features at around 324 and 400 nm. To interpret these absorption features, we simulated the optical absorption spectra of the $[Au_{22}H_3]^{3+}$ and $[Au_{11}]^{3+}$ clusters using time-dependent density functional theory (TD-DFT). Overall, good agreement between the experiment and the simulation has been found for both clusters (Figure S18a, 18b). For $[Au_{22}H_3]^{3+}$, the 323 nm band involves many close excitations of Au d → sp (Table S2), the 394 nm band is assigned mainly to the HOMO−7 → LUMO+1 transition (Au d/s → sp excitation), and the 446 nm band is assigned to HOMO → LUMO+9 transition (Au sp → p excitation). The frontier orbitals of $[Au_{22}H_3]^{3+}$ involved in the transitions all show features along the rod-shaped structure of the cluster (Figure S18c). For comparison, the 324 nm band of the $[Au_{11}]^{3+}$ cluster also involves many close excitations of mainly Au d → p (Table S3), while its 400 nm band has just a few strong transitions (Au sp → sp). The ligands are more involved in the frontier orbitals of the $[Au_{11}]^{3+}$ cluster (Figure S18d). The results indicate that the Au_{22} core in $[Au_{22}H_3]^{3+}$ may also be composed of two Au_{11} units bonded via Au atoms and the Au_{11} units may have similar structures with the $[Au_{11}]^{3+}$ cluster.

The stability of a high purity $[Au_{22}H_3]^{3+}$ sample in solid state was tested at ambient conditions. The UV−vis absorption spectra were measured and compared after six months (Figure 2d). The three main absorption features remain prominent

https://doi.org/10.1021/jacs.2c00725
J. Am. Chem. Soc. 2022, 144, 5258−5262

with only a slight decrease, suggesting the mixed ligand Au nanohydride cluster is very stable. The ESI mass spectra in Figure S5 also agree well with the absorption spectra, confirming its high stability in the solid state, even though the cluster is less stable in solution (Figure S8).

We studied the surface redox properties and CO_2RR activities of $[Au_{22}H_3]^{3+}$, in comparison with those of $[Au_{11}]^{3+}$. We first tested the cyclic voltammetry (CV) of the two clusters, as shown in Figure S9. It demonstrates that the existence of H atoms in the $[Au_{22}H_3]^{3+}$ cluster leads to a unique oxidation peak at 0.88 V and shifts the Au(I)/Au(0) reduction peak from 1.02 to 1.05 V relative to $[Au_{11}]^{3+}$. Figures S10 and S11 show the CVs of $[Au_{22}H_3]^{3+}$ and $[Au_{11}]^{3+}$ in N_2- and CO_2-saturated 0.5 M $KHCO_3$. The current density starts to increase as the potential reaches approximately −0.3 V in the N_2-saturated electrolyte, due to the hydrogen evolution reaction (HER) and CO_2RR. Both clusters have higher current densities in CO_2-saturated solution under the same potential, indicating both samples can effectively catalyze the electroreduction of CO_2. The electrocatalytic reduction of CO_2 was studied by linear sweep voltammetry (LSV) in the CO_2-saturated 0.5 M $KHCO_3$ (Figure 3a) to obtain the potentials required to reduce CO_2. The $[Au_{22}H_3]^{3+}$ cluster shows a lower onset potential and higher current density relative to $[Au_{11}]^{3+}$. In the subsequent electrolysis test at a constant potential, only H_2 and CO were detected in all our expeirments (as described in the SI and Figure S12). Figure 3b compares the potential dependent FEs for the formation of CO over $[Au_{22}H_3]^{3+}$ and $[Au_{11}]^{3+}$. We found that the $[Au_{22}H_3]^{3+}$ cluster shows higher FE toward CO than the $[Au_{11}]^{3+}$ cluster under all voltages. When more negative potentials are applied, the FE first increases and then decreases, reaching a maximum at about −0.6 V. This trend is similar to the recently reported phosphine/thiolate coprotected Au_{55} cluster.[45] The best catalytic performance of $[Au_{22}H_3]^{3+}$ was observed at −0.6 V with an FE_{CO} of 92.7%, which is significantly higher than that of the thiolate-protected Au_{25} cluster at a similar potential.[27] Furthermore, the $[Au_{22}H_3]^{3+}$ cluster also shows a very high turnover frequency (TOF) of 488 h^{-1} and mass activity of 134 A/g_{Au} at −0.6 V (Figure 3c and 3d), which is much higher than the values of Au nanoparticles[6−9] at the same potential due to the higher ratio of surface atoms. For comparison, the $[Au_{11}]^{3+}$ cluster has an FE_{CO} of 70.6% at −0.6 V, which is close to the reported value for $[Au_{11}(PPh_3)_8Cl_2]^+$.[46] Relative to that of $[Au_{22}H_3]^{3+}$, the current densities of $[Au_{11}]^{3+}$ at all potentials are lower (Figure S13). In addition, the TOF value of 276 h^{-1} and mass activity of 75.8 A/g_{Au} at −0.6 V suggest a much lower activity of the $[Au_{11}]^{3+}$ cluster than the $[Au_{22}H_3]^{3+}$ cluster.

It is noteworthy that the $[Au_{22}H_3]^{3+}$ cluster not only exhibits promising selectivity and activity toward CO_2RR but also remains stable during the electrochemical CO_2RR. The stability test results in Figure 3e indicate the current density stays steady at −3.5 $mAcm^{-2}$ during the 10 h electrolysis at −0.6 V, with the FE_{CO} only dropping slightly (5.6%). It is also confirmed with XPS analysis before and after the electrolysis, as shown in Figure S17. The performance of the $[Au_{22}H_3]^{3+}$ electrode was measured after one month of storage in air; the FE_{CO} at −0.6 V only drops 3.4% (Figure S16). All these results prove that the $[Au_{22}H_3]^{3+}$ cluster is a stable CO_2RR catalyst.

DFT calculations were carried out to understand the mechanisms of the CO_2RR on $[Au_{22}H_3]^{3+}$; the reaction pathways for the two nanoclusters are shown in Figure 4. We found that the bridge H atom in $[Au_{22}H_3]^{3+}$ could directly

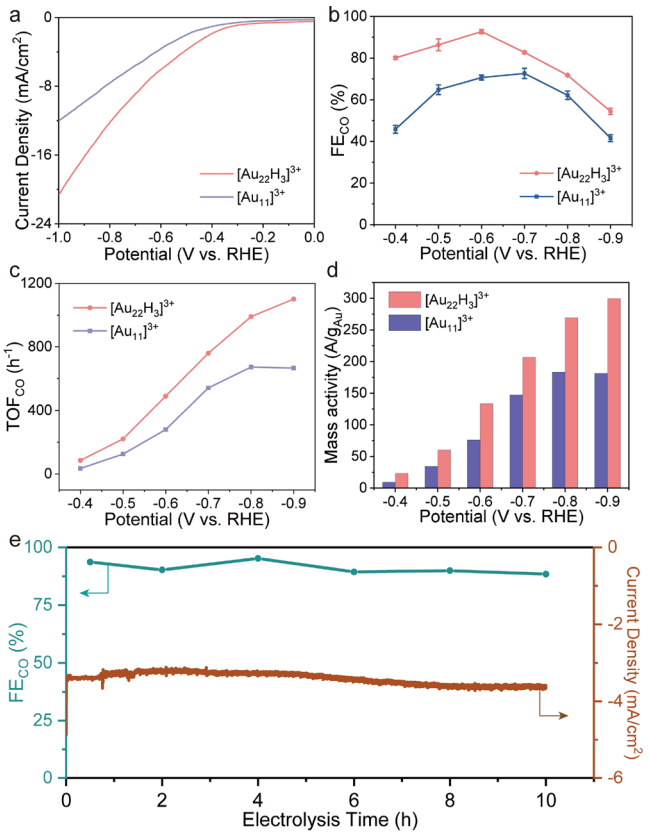

Figure 3. Selectivity, activity, and stability of $[Au_{22}H_3]^{3+}$ and $[Au_{11}]^{3+}$ in the electrocatalytic reduction of CO_2 to CO. (a) LSV curves. (b) FE_{CO} and (c) TOF_{CO} of the two clusters. (d) Potential-dependent mass activity of the two clusters. (e) Stability test of $[Au_{22}H_3]^{3+}$ for electrolysis at −0.6 V.

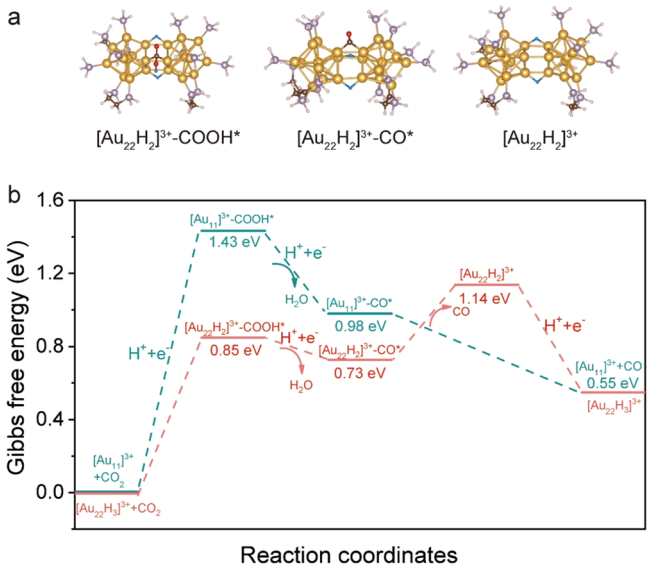

Figure 4. DFT structures and energetics of CO_2RR. (a) Optimized structures of the intermediates on $[Au_{22}H_3]^{3+}$ for *COOH and *CO and after CO desorption. Color code: Au = yellow; C = brown; *P* = purple; Hydride = blue; H on the ligands = white; O = red. (b) Free energy profiles of CO_2RR on the $[Au_{11}]^{3+}$ (cyan lines) and $[Au_{22}H_3]^{3+}$ (red lines) clusters at 0 V vs RHE.

https://doi.org/10.1021/jacs.2c00725
J. Am. Chem. Soc. 2022, 144, 5258−5262

hydrogenate CO_2 to form adsorbed *COOH (Figure 4a) with a Gibbs free energy (ΔG) change of 0.85 eV (Figure 4b). Then, an electrochemical proton reduction process takes place on *COOH, leading to the formation of adsorbed CO* and H_2O. Although CO desorption has a higher barrier on $[Au_{22}H_2]^{3+}$ than on $[Au_{11}]^{3+}$, the formation of the key *COOH intermediate is much more difficult on $[Au_{11}]^{3+}$ than on $[Au_{22}H_2]^{3+}$. This is because the $[Au_{11}]^{3+}$ cluster requires proton reduction from the electrolyte to form COOH* (Figure S19). As a result, the DFT profiles in Figure 4b indicate that it is much more favorable to form CO on $[Au_{22}H_2]^{3+}$ than on $[Au_{11}]^{3+}$, in agreement with our experimental observations (Figure 3). Moreover, Figure 4b shows that the H vacancy in $[Au_{22}H_2]^{3+}$ can be readily recovered by proton reduction (Figure S20), completing the catalytic cycle. Although the CO_2RR pathway on $[Au_{22}H_3]^{3+}$ shown in Figure 4b resembles the lattice hydride mechanism of CO_2RR on copper hydride nanoclusters,[47] an important difference is in selectivity, because HCOOH is preferred over CO on the latter. We have also computed the ΔG for HCOOH formation via hydride addition and the *HCOO intermediate on $[Au_{22}H_2]^{3+}$ but found that it is less favorable than CO formation (Figure S21). In other words, the lattice hydrides in $[Au_{22}H_3]^{3+}$ behave very differently from those in the Cu−H systems.

In conclusion, we have synthesized a new heteroleptic Au trihydride nanocluster, $[Au_{22}H_3(dppe)_3(PPh_3)_8]^{3+}$. The use of the mixed ligands provides the cluster with both Au−H active sites and good stability. The cluster is found to be an excellent electrochemical CO_2RR catalyst, which exhibits high reactivity and selectivity to CO (92.7% FE and 134 A/g_{Au} mass activity at −0.6 V) and long-term stability. DFT studies of the CO_2RR mechanisms revealed that the Au nanohydride cluster facilitates the formation of the key *COOH intermediate, thereby favoring the CO product. The current work uncovers a unique Au nanohydride cluster with well-defiend *in situ* catalytic centers for CO_2RR and suggests new approaches to design nanocatalysts for understanding structure−activity relationships and energy applications.

■ ASSOCIATED CONTENT

Supporting Information

The Supporting Information is available free of charge at https://pubs.acs.org/doi/10.1021/jacs.2c00725.

Experimental methods, analyses of Au nanoclusters and their electrocatalysis, and computational details (PDF)

■ AUTHOR INFORMATION

Corresponding Authors

De-en Jiang − *Department of Chemistry, University of California, Riverside, California 92521, United States;* orcid.org/0000-0001-5167-0731; Email: djiang@ucr.edu

Shouheng Sun − *Department of Chemistry, Brown University, Providence, Rhode Island 02912, United States;* orcid.org/0000-0002-4051-0430; Email: shouheng_sun@brown.edu

Lai-Sheng Wang − *Department of Chemistry, Brown University, Providence, Rhode Island 02912, United States;* orcid.org/0000-0003-1816-5738; Email: lai-sheng_wang@brown.edu

Authors

Ze-Hua Gao − *Department of Chemistry, Brown University, Providence, Rhode Island 02912, United States*

Kecheng Wei − *Department of Chemistry, Brown University, Providence, Rhode Island 02912, United States*

Tao Wu − *Department of Chemistry, University of California, Riverside, California 92521, United States*

Jia Dong − *Department of Chemistry, Brown University, Providence, Rhode Island 02912, United States;* orcid.org/0000-0001-7711-1655

Complete contact information is available at: https://pubs.acs.org/10.1021/jacs.2c00725

Notes

The authors declare no competing financial interest.

■ ACKNOWLEDGMENTS

We thank Dr. T. L. Shen for help with the ESI-MS experiments and Dr. R. Hopson for help with the NMR experiments. This research was supported by a seed grant from the Office of the Vice President for Research at Brown University (to L.S.W.) and the NSF under Grant CHE-2102290 (to S.H.S.). The DFT computation was supported by the U.S. Department of Energy, Office of Science, Office of Basic Energy Sciences, Chemical Sciences, Geosciences, and Biosciences Division, Catalysis Science Program (to D.E.J.).

■ REFERENCES

(1) Turner, J. A. A Realizable Renewable Energy Future. *Science* **1999**, *285*, 687−689.

(2) De Luna, P.; Hahn, C.; Higgins, D.; Jaffer, S. A.; Jaramillo, T. F.; Sargent, E. H. What Would It Take for Renewably Powered Electrosynthesis to Displace Petrochemical Processes? *Science* **2019**, *364*, 350.

(3) Hori, Y.; Murata, A.; Kikuchi, K.; Suzuki, S. Electrochemical Reduction of Carbon Dioxides to Carbon Monoxide at a Gold Electrode in Aqueous Potassium Hydrogen Carbonate. *J. Chem. Soc., Chem. Commun.* **1987**, *10*, 728−729.

(4) Wang, G.; Chen, J.; Ding, Y.; Cai, P.; Yi, L.; Li, Y.; Tu, C.; Hou, Y.; Wen, Z.; Dai, L. Electrocatalysis for CO_2 Conversion: From Fundamentals to Value-Added Products. *Chem. Soc. Rev.* **2021**, *50*, 4993−5061.

(5) Haruta, M. Size-and Support-Dependency in the Catalysis of Gold. *Catal. Today* **1997**, *36*, 153−166.

(6) Zhu, W.; Michalsky, R.; Metin, O.; Lv, H.; Guo, S.; Wright, C. J.; Sun, X.; Peterson, A. A.; Sun, S. Monodisperse Au Nanoparticles for Selective Electrocatalytic Reduction of CO_2 to CO. *J. Am. Chem. Soc.* **2013**, *135*, 16833−16836.

(7) Mistry, H.; Reske, R.; Zeng, Z.; Zhao, Z. J.; Greeley, J.; Strasser, P.; Cuenya, B. R. Exceptional Size-Dependent Activity Enhancement in the Electroreduction of CO_2 over Au Nanoparticles. *J. Am. Chem. Soc.* **2014**, *136*, 16473−16476.

(8) Zhu, W.; Zhang, Y. J.; Zhang, H.; Lv, H.; Li, Q.; Michalsky, R.; Peterson, A. A.; Sun, S. Active and Selective Conversion of CO_2 to CO on Ultrathin Au Nanowires. *J. Am. Chem. Soc.* **2014**, *136*, 16132−16135.

(9) Souza, M. L.; Lima, F. H. Dibenzyldithiocarbamate-Functionalized Small Gold Nanoparticles as Selective Catalysts for the Electrochemical Reduction of CO_2 to CO. *ACS Catal.* **2021**, *11*, 12208−12219.

(10) Chakraborty, I.; Pradeep, T. Atomically Precise Clusters of Noble Metals: Emerging Link between Atoms and Nanoparticles. *Chem. Rev.* **2017**, *117*, 8208−8271.

(11) Naveen, M. H.; Khan, R.; Bang, J. H. Gold Nanoclusters as Electrocatalysts: Atomic Level Understanding from Fundamentals to Applications. *Chem. Mater.* **2021**, *33*, 7595−7612.

(12) Levi-Kalisman, Y.; Jadzinsky, P. D.; Kalisman, N.; Tsunoyama, H.; Tsukuda, T.; Bushnell, D. A.; Kornberg, R. D. Synthesis and Characterization of $Au_{102}(p\text{-MBA})_{44}$ Nanoparticles. *J. Am. Chem. Soc.* **2011**, *133*, 2976−2982.
(13) Li, G.; Jin, R. Atomically Precise Gold Nanoclusters as New Model Catalysts. *Acc. Chem. Res.* **2013**, *46*, 1749−1758.
(14) Jin, R.; Zeng, C.; Zhou, M.; Chen, Y. Atomically Precise Colloidal Metal Nanoclusters and Nanoparticles: Fundamentals and Opportunities. *Chem. Rev.* **2016**, *116*, 10346−103413.
(15) Yan, N.; Xia, N.; Liao, L.; Zhu, M.; Jin, F.; Jin, R.; Wu, Z. Unraveling the Long-Pursued Au_{144} Structure by X-Ray Crystallography. *Sci. Adv.* **2018**, *4*, No. eaat7259.
(16) Zhu, M.; Aikens, C. M.; Hollander, F. J.; Schatz, G. C.; Jin, R. Correlating the Crystal Structure of a Thiol-Protected Au_{25} cluster and Optical Properties. *J. Am. Chem. Soc.* **2008**, *130*, 5883−5885.
(17) Negishi, Y.; Nakazaki, T.; Malola, S.; Takano, S.; Niihori, Y.; Kurashige, W.; Yamazoe, S.; Tsukuda, T.; Hakkinen, H. A Critical Size for Emergence of Nonbulk Electronic and Geometric Structures in Dodecanethiolate-Protected Au Clusters. *J. Am. Chem. Soc.* **2015**, *137*, 1206−1212.
(18) Zeng, C.; Chen, Y.; Liu, C.; Nobusada, K.; Rosi, N. L.; Jin, R. Gold Tetrahedra Coil Up: Kekule-like and Double Helical Superstructures. *Sci. Adv.* **2015**, *1*, No. e1500425.
(19) Konishi, K.; Iwasaki, M.; Shichibu, Y. Phosphine-Ligated Gold Clusters with Core+Exo Geometries: Unique Properties and Interactions at the Ligand-Cluster Interface. *Acc. Chem. Res.* **2018**, *51*, 3125−3133.
(20) Yuan, S. F.; Xu, C. Q.; Li, J.; Wang, Q. M. A Ligand-Protected Golden Fullerene: The Dipyridylamido Au_{32}^{8+} Nanocluster. *Angew. Chem., Int. Ed.* **2019**, *58*, 5906−5909.
(21) Kang, X.; Wei, X.; Liu, X.; Wang, S.; Yao, T.; Wang, S.; Zhu, M. A Reasonable Approach for the Generation of Hollow Icosahedral Kernels in Metal Nanoclusters. *Nat. Commun.* **2021**, *12*, 6186.
(22) Wu, Z.; Hu, G.; Jiang, D.-e.; Mullins, D. R.; Zhang, Q. F.; Allard, L. F., Jr; Wang, L. S.; Overbury, S. H. Diphosphine-Protected Au_{22} Nanoclusters on Oxide Supports Are Cctive for Gas-Phase Catalysis without Ligand Removal. *Nano Lett.* **2016**, *16*, 6560−6567.
(23) Kwak, K.; Lee, D. Electrochemistry of Atomically Precise Metal Nanoclusters. *Acc. Chem. Res.* **2019**, *52*, 12−22.
(24) Cai, X.; Hu, W.; Xu, S.; Yang, D.; Chen, M.; Shu, M.; Si, R.; Ding, W.; Zhu, Y. Structural Relaxation Enabled by Internal Vacancy Available in a 24-Atom Gold Cluster Reinforces Catalytic Reactivity. *J. Am. Chem. Soc.* **2020**, *142*, 4141−4153.
(25) Hasegawa, S.; Takano, S.; Harano, K.; Tsukuda, T. New Magic Au_{24} Cluster Stabilized by PVP: Selective Formation, Atomic Structure, and Oxidation Catalysis. *JACS Au* **2021**, *1*, 660−668.
(26) Kauffman, D. R.; Alfonso, D.; Matranga, C.; Qian, H.; Jin, R. Experimental and Computational Investigation of Au_{25} Clusters and CO_2: A Unique Interaction and Enhanced Electrocatalytic Activity. *J. Am. Chem. Soc.* **2012**, *134*, 10237−10243.
(27) Zhao, S.; Austin, N.; Li, M.; Song, Y.; House, S. D.; Bernhard, S.; Yang, J. C.; Mpourmpakis, G.; Jin, R. Influence of Atomic-level Morphology on Catalysis: The Case of Sphere and Rod-like Gold Nanoclusters for CO_2 Electroreduction. *ACS Catal.* **2018**, *8*, 4996−5001.
(28) Li, S.; Alfonso, D.; Nagarajan, A. V.; House, S. D.; Yang, J. C.; Kauffman, D. R.; Mpourmpakis, G.; Jin, R. Monopalladium Substitution in Gold Nanoclusters Enhances CO_2 Electroreduction Activity and Selectivity. *ACS Catal.* **2020**, *10*, 12011−12016.
(29) Seong, H.; Efremov, V.; Park, G.; Kim, H.; Yoo, J. S.; Lee, D. Atomically Precise Gold Nanoclusters as Model Catalysts for Identifying Active Sites for Electroreduction of CO_2. *Angew. Chem., Int. Ed.* **2021**, *60*, 14563−14570.
(30) Li, S.; Nagarajan, A. V.; Alfonso, D. R.; Sun, M.; Kauffman, D. R.; Mpourmpakis, G.; Jin, R. Boosting CO_2 Electrochemical Reduction with Atomically Precise Surface Modification on Gold Nanoclusters. *Angew. Chem., Int. Ed.* **2021**, *60*, 6351−6356.
(31) Alfonso, D. R.; Kauffman, D.; Matranga, C. Active Sites of Ligand-Protected Au_{25} Nanoparticle Catalysts for CO_2 Electroreduction to CO. *J. Chem. Phys.* **2016**, *144*, 184705.
(32) Li, J.; Li, X.; Zhai, H. J.; Wang, L. S. Au_{20}: A Tetrahedral Cluster. *Science* **2003**, *299*, 864−867.
(33) Zhang, H. F.; Stender, M.; Zhang, R.; Wang, C.; Li, J.; Wang, L. S. Toward the Solution Synthesis of the Tetrahedral Au_{20} Cluster. *J. Phys. Chem. B* **2004**, *108*, 12259−12263.
(34) Chen, J.; Zhang, Q. F.; Williard, P. G.; Wang, L. S. Synthesis and Structure Determination of a New Au_{20} Nanocluster Protected by Tripodal Tetraphosphine Ligands. *Inorg. Chem.* **2014**, *53*, 3932−3934.
(35) Zhang, Q.-F.; Chen, X.; Wang, L. S. Toward Solution Syntheses of the Tetrahedral Au_{20} Pyramid and Atomically Precise Gold Nanoclusters with Uncoordinated Sites. *Acc. Chem. Res.* **2018**, *51*, 2159−2168.
(36) Chen, J.; Zhang, Q. F.; Bonaccorso, T. A.; Williard, P. G.; Wang, L. S. Controlling Gold Nanoclusters by Diphosphine Ligands. *J. Am. Chem. Soc.* **2014**, *136*, 92−95.
(37) Hu, G.; Wu, Z.; Jiang, D. E. Stronger-Than-Pt Hydrogen Adsorption in a Au_{22} Nanocluster for the Hydrogen Evolution Reaction. *J. Mater. Chem. A* **2018**, *6*, 7532−7537.
(38) Dong, J.; Gao, Z. H.; Zhang, Q. F.; Wang, L. S. The Synthesis, Bonding, and Transformation of a Ligand-Protected Gold Nanohydride Cluster. *Angew. Chem., Int. Ed.* **2021**, *60*, 2424−2430.
(39) Dong, J.; Gao, Z. H.; Wang, L. S. The Synthesis and Characterization of a New Diphosphine-Protected Gold Hydride Nanocluster. *J. Chem. Phys.* **2021**, *155*, 034307.
(40) de Silva, N.; Ha, J. M.; Solovyov, A.; Nigra, M. M.; Ogino, I.; Yeh, S. W.; Durkin, K. A.; Katz, A. A Bioinspired Approach for Controlling Accessibility in Calix[4]arene-bound Metal Cluster Catalysts. *Nat. Chem.* **2010**, *2*, 1062−1068.
(41) Das, A.; Li, T.; Nobusada, K.; Zeng, Q.; Rosi, N. L.; Jin, R. Total Structure and Optical Properties of a Phosphine/Thiolate-Protected Au_{24} Nanocluster. *J. Am. Chem. Soc.* **2012**, *134*, 20286−20289.
(42) Yuan, S. F.; Lei, Z.; Guan, Z. J.; Wang, Q. M. Atomically Precise Preorganization of Open Metal Sites on Gold Nanoclusters with High Catalytic Performance. *Angew. Chem., Int. Ed.* **2021**, *60*, 5225−5229.
(43) Wang, X.; Wang, S.; Qian, S.; Liu, N.; Dou, X.; Yuan, X. Mechanistic Insights into the Two-phase Synthesis of Heteroleptic Au Nanoclusters. *Nanoscale* **2021**, *13*, 3512−3518.
(44) Takano, S.; Hirai, H.; Muramatsu, S.; Tsukuda, T. Hydride-Doped Gold Superatom $(Au_9H)^{2+}$: Synthesis, Structure, and Transformation. *J. Am. Chem. Soc.* **2018**, *140*, 8380−8383.
(45) Wan, X. K.; Wang, J. Q.; Wang, Q. M. J. A. C. Ligand-Protected Au_{55} with a Novel Structure and Remarkable CO_2 Electroreduction Performance. *Angew. Chem., Int. Ed.* **2021**, *60*, 20748−20753.
(46) Narouz, M. R.; Osten, K. M.; Unsworth, P. J.; Man, R. W. Y.; Salorinne, K.; Takano, S.; Tomihara, R.; Kaappa, S.; Malola, S.; Dinh, C. T.; Padmos, J. D.; Ayoo, K.; Garrett, P. J.; Nambo, M.; Horton, J. H.; Sargent, E. H.; Hakkinen, H.; Tsukuda, T.; Crudden, C. M. N-Heterocyclic Carbene-Functionalized Magic Number Gold Nanoclusters. *Nat. Chem.* **2019**, *11*, 419−425.
(47) Tang, Q.; Lee, Y.; Li, D. Y.; Choi, W.; Liu, C. W.; Lee, D.; Jiang, D. E. Lattice-hydride Mechanism in Electrocatalytic CO_2 Reduction by Structurally Precise Copper-Hydride Nanoclusters. *J. Am. Chem. Soc.* **2017**, *139*, 9728−9736.

https://doi.org/10.1021/jacs.2c00725
J. Am. Chem. Soc. 2022, 144, 5258−5262